Overview

Electronic properties and charge carrier mobilities of graphynes and graphdiynes from first principles

Jinyang Xi, Dong Wang and Zhigang Shuai*

The sp^1+sp^2 hybridized carbon allotropes, graphynes (GYs) and graphdiynes (GDYs), have attracted increased attention, and researches from both theoretical and experimental communities are emerging. Theoretical calculations show that the electronic properties of GYs and GDYs can be tuned by straining, cutting into nanoribbons with different widths and edge morphology, and applying external electric fields. Due to their unique electronic properties, GYs and GDYs exhibit charge carrier mobility as high as ~10^4–10^5 $cm^2\,V^{-1}$ $second^{-1}$ at room temperature based on the first-principle calculations and the Boltzmann transport equation. Interestingly, the charge carrier mobility in 6,6,12-GY with double Dirac cone structure is found to be even larger than that in graphene at room temperature. Through an in-depth description of electron–phonon couplings by density functional perturbation theory, it is suggested that the intrinsic charge carrier transport in these carbon allotropes is dominated by the longitudinal acoustic phonon scatterings over a wide range of temperatures, although scatterings with optical phonon modes cannot be neglected at high temperatures. The unique electronic properties of GYs and GDYs make them highly promising for applications in next generation nanoelectronics.

How to cite this article:
WIREs Comput Mol Sci 2015, 5:215–227. doi: 10.1002/wcms.1213

INTRODUCTION

Carbon possesses several allotropes, such as fullerenes,[1] nanotubes,[2] and graphene.[3] These allotropes exhibit unique mechanical, electronic, and electrochemical properties, and have been considered as potential low-dimensional materials for nanoelectronics, chemical sensors, and energy storage.[4–6] Recently, the new forms of two-dimensional (2D) carbon allotropes, graphynes (GYs) and graphdiynes (GDYs), consisting of one layer of *sp*- and sp^2-hybridized carbon atoms, have caught great attention due to their graphene-like structures and intriguing electronic, optical, and mechanical properties.[7,8] The structure of GYs is formed by inserting C≡C triple bonds into the honeycomb lattice of graphene, and it takes three typical forms: *α*-, *β*-, and *γ*-GYs (Figure 1(a)–(c)), as first proposed theoretically by Baughman et al. in 1987.[9] The building blocks of GDY (Figure 1(d)), which can be constructed by inserting diacetylenic linkages C≡C—C≡C into the lattice of graphene, were synthesized in 1997 by Haley et al.[10] In 2010, Li et al. have, for the first time, synthesized large-area GDY films on Cu surface by a cross-coupling reaction, and the room temperature conductivity was measured to be 2.516×10^{-4} Sm^{-1}.[11] Then, in 2012, they fabricated one-dimensional (1D) GDY nanowires with high conductivity (1.9×10^3 Sm^{-1}) and mobility (7.1×10^2 $cm^2\,V^{-1}$ $second^{-1}$) at room temperature.[12] These experiments demonstrated GDYs to be attractive electronic materials. First-principle calculations show that GDY is a semiconductor[13–15] and some GYs (such as *α*-, *β*-, and 6,6,12-GYs) have Dirac cones just like graphene (Figure 1(e) shows the structure of 6,6,12-GY).[16,17] Meanwhile, it has been

*Correspondence to: zgshuai@tsinghua.edu.cn

MOE Key Laboratory of Organic OptoElectronics and Molecular Engineering, Department of Chemistry, Tsinghua University, Beijing, P.R. China

Conflict of interest: The authors have declared no conflicts of interest for this article.

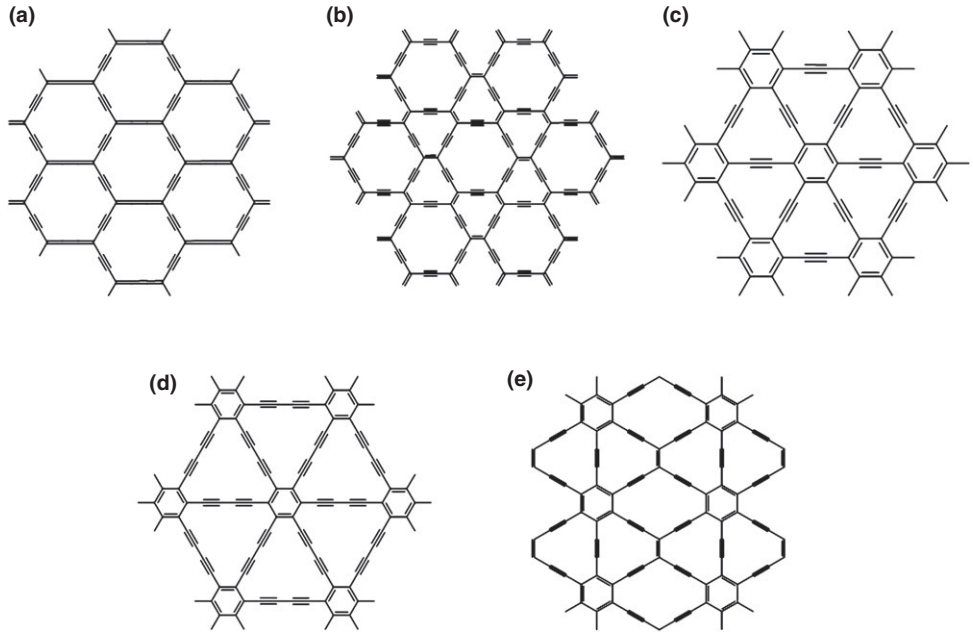

FIGURE 1 | Geometric structures of (a) α-graphyne (GY), (b) β-GY, (c) γ-GY, (d) graphdiynes (GDY), and (e) 6,6,12-GY.

shown that the band gaps of GYs and GDYs can be tuned by strain,[18,19] cutting into nanoribbons (NRs) with different widths and edge morphology,[20–22] external electric fields,[23–25] etc. The charge carrier mobility in these carbon allotropes is predicted to be as high as $\sim 10^4$–10^5 $cm^2\ V^{-1}\ second^{-1}$ at room temperature.[21,22,26] Interestingly, the charge carrier mobility in 6,6,12-GY with double Dirac cone structure is found to be even larger than that in graphene.[27]

We noticed there have been some comprehensive reviews about GYs and GDYs,[7,8,28] in this overview, we focused on the recent theoretical predictions of electronic structures of GYs, GDYs, and 1D NRs and the charge transport behavior. Particularly, we discuss the key factors in determining the intrinsic carrier mobility, electron–phonon couplings (EPCs), based on the deformation potential (DP) theory and density functional perturbation theory (DFPT), respectively.

ELECTRONIC STRUCTURES

2D GY and GDY Sheets

Both γ-GY and GDY are calculated to be direct-band-gap semiconductors, at the **M** and **Γ** points of the first Brillouin zone, respectively. The band gaps of these two carbon allotropes have been estimated to fall into a wide range (0.47–2.23 eV[9,14,29,30] for γ-GY and 0.44–1.22 eV[13–15,22,30] for GDY) depending on the methods and the exchange-correlation functionals, as summarized in Table 1. The band structures by the Perdew, Burke, and Ernzerhof (PBE) functional of γ-GY and GDY[30] are shown in Figure 2(a) and (b), respectively. The natural band gaps of γ-GY and GDY facilitate their applications in photoelectronic devices. Unlike γ-GY and GDY, α- and β-GYs are both gapless with one Dirac cone at the **K** point[27] (Figure 2(c) and (d), respectively). Recently, Görling et al.[17] demonstrated that the existence of Dirac cones is not a unique feature of the hexagonal symmetry structure (e.g., graphene, α-, and β-GYs). They found that 6,6,12-GY, which has rectangular symmetry, features two self-doped non-equivalent and distorted Dirac cones (Figure 2(e)). This finding suggests that electronic properties of 6,6,12-GY are even more amazing than graphene.

The first-principle calculations predicted that the band structures of GYs and GDY can be tuned by

TABLE 1 | The Band Gaps (E_g) of γ-Graphyne (GY) and Graphdiyne (GDY) from Different Theoretical Methods, Respectively

	γ-GY	GDY
E_g/method	1.2 eV/MNDO[9]	0.44 eV/LDA[13]
	0.52 eV/FP-LCAO[14]	1.10 eV/GW[13]
	0.47 eV/PBE[29,30]	0.53 eV/FP-LCAO[14]
	2.23 eV/B3LYP[30]	1.22 eV/HSE06[15]
		0.46 eV/PBE[22]
		0.52 eV/PBE[30]
		1.18 eV/B3LYP[30]

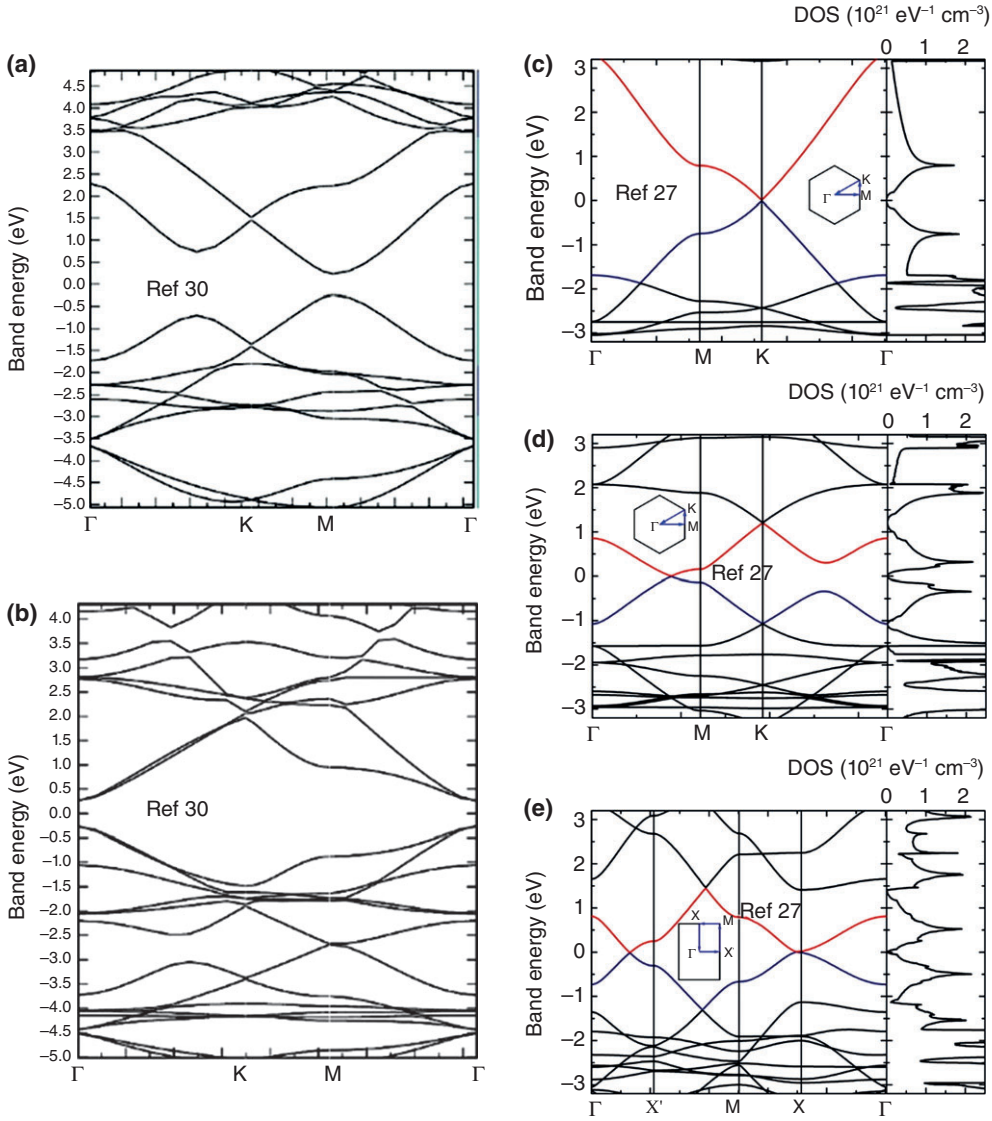

FIGURE 2 | Band structures of (a) γ-graphyne (GY) and (b) graphdiynes (GDY) at the Perdew, Burke, and Ernzerhof (PBE) level. (Reprinted with permission from Ref 30. Copyright 2012 American Chemical Society); Band structure and density of states (DOS) of (c) α-, (d) β-, and (e) 6,6,12-GYs at the PBE level. (Reprinted with permission from Ref 27. Copyright 2013 American Chemical Society)

strains. Su et al.[18] showed that at the PW91 level, the band gap of GDY increases from 0.47 to 1.39 eV with increasing the biaxial tensile strain, while it decreases from 0.47 eV to nearly zero with increasing the uniaxial tensile strain, resulting from the break of the geometrical symmetry. For γ-GY, Li et al.[19] demonstrated that the direct-band-gap character is maintained, but the magnitude of band gap is tunable under strains. In case of tensile strain, the band gap increases as the strain increases, whereas it decreases under the compressive strain from both PBE and HSE06 calculations. Furthermore, they found that the band gaps of the GY family can be modulated through different types of strain. These results suggest that GYs and GDY are potential materials for strain-tunable nanoelectronics and optoelectronics devices, as well as sensors.

With the progress in the study of the monolayer GYs and GDY, people also turned their attention to the few-layer systems of these carbon allotropes. Leenaerts et al.[25] have studied the bilayer α-GY from the first-principle calculations and found that its band structure is qualitatively different from its monolayer form and depends critically on the stacking mode of the two layers. For the stable AB stacking mode (Figure 3(a)), it exhibits a gapless parabolic band structure (Figure 3(b)), similar to the AB stacking bilayer graphene; for the other stable AB stacking

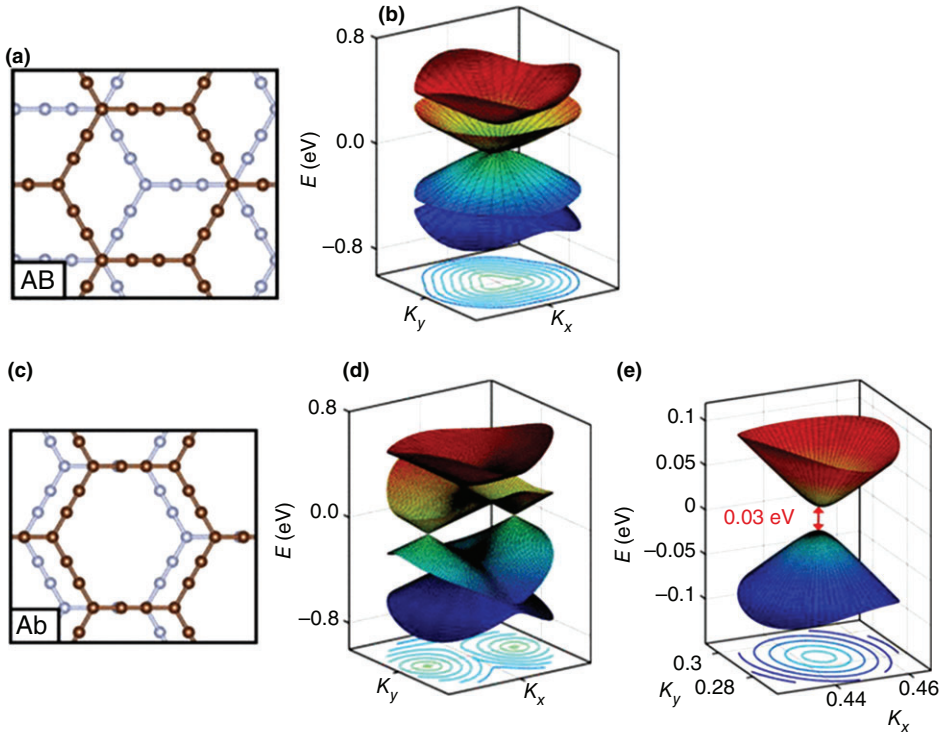

FIGURE 3 | Two most stable stacking configurations for bilayer α-graphyne (GY): (a) AB stacking and (b) its gapless parabolic band structure, (c) Ab stacking and its Dirac cone in the absence (d) and presence (e) of an electric field (0.1 VÅ^{-1}). (Reprinted with permission from Ref 25. Copyright 2013 AIP Publishing LLC)

mode (Figure 3(c)), it exhibits a double Dirac cone spectrum (Figure 3(d)) and the band gap can be tuned by an electric field (a gap opening of 0.03 eV at the electric field of 0.1 VÅ^{-1}, Figure 3(e)). For few-layer GDYs, Lu et al.[24] reported that the most stable bilayer and trilayer GDYs both have their hexagonal rings stacked in a Bernal way (AB and ABA style configurations, respectively, as shown in Figure 4). Based on the PW91 calculations, the band gaps of the most stable stacking configurations for bilayer and trilayer GDYs are 0.35 eV (direct band gap, Figure 4(a)) and 0.33 eV (indirect band gap, Figure 4(b)), respectively. Both values are smaller than that of the monolayer GDY (0.46 eV) due to the interlayer interactions. Interestingly, the band gaps of the semiconducting bilayer and trilayer GDYs generally decrease with increasing the external vertical electric field, irrespective of the stacking style. In addition to the tunable band gaps of few-layer GYs and GDYs, the theoretical calculations find that bulk γ-GY and GDY can be either metallic or semiconducting, depending on the stacking arrangements (e.g., for AB stacking styles, the band gaps can be ~0.5 eV at LSDA level for bulk γ-GY[31] and ~0.74 eV at HSE06 level for bulk GDY,[32] respectively, while both are metals for AA stacking style). Therefore, it is possible to tune the electronic structures and optical absorptions of few-layer GYs and GDYs with an external electric field.

1D Graphyne and Graphdiyne Nanoribbons

It has been established that the band gap of graphene can be engineered by cutting the graphene sheet into NRs with different widths, edge morphology, edge functionalization, etc.[33] Similarly, these band gap engineering methods are expected to be applicable to GYs and GDYs. Very recently, several theoretical works have been conducted to understand the basic properties of NRs of GYs and GDY.[20–22] Just like graphene, cutting through infinite γ-GY and GDY sheet along two directions indicated as X and Y, one can obtain armchair nanoribbons (ANRs) and zigzag nanoribbons (ZNRs) of various widths, as depicted in Figure 5. The index n in Figure 5 indicates the number of the repeating units along the direction of the NR width. Unlike ANRs, in ZNRs the number of n can differ by a half-integer. Du et al.[20] have studied the γ-GY and GDY ANRs and ZNRs with variable widths by using the local density approximation (LDA) functional. They found that all the γ-GY and GDY NRs are semiconductors and the band gaps decrease as the widths of NRs increase, with the band gaps ranging

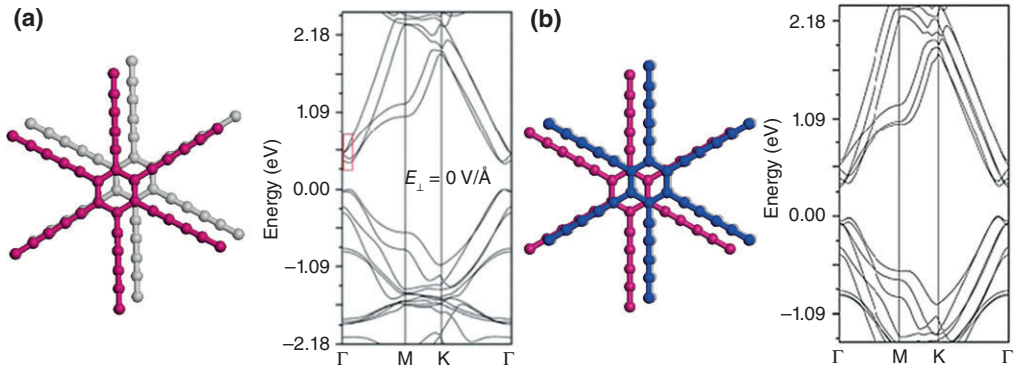

FIGURE 4 | (a) The most stable configuration of bilayer graphdiynes (GDY) AB (β_1) and the band structure without electric field; (b) ABA configuration of trilayer GDY and the band structure without electric field. (Reproduced with permission from Ref 24. Copyright 2012 The Royal Society of Chemistry)

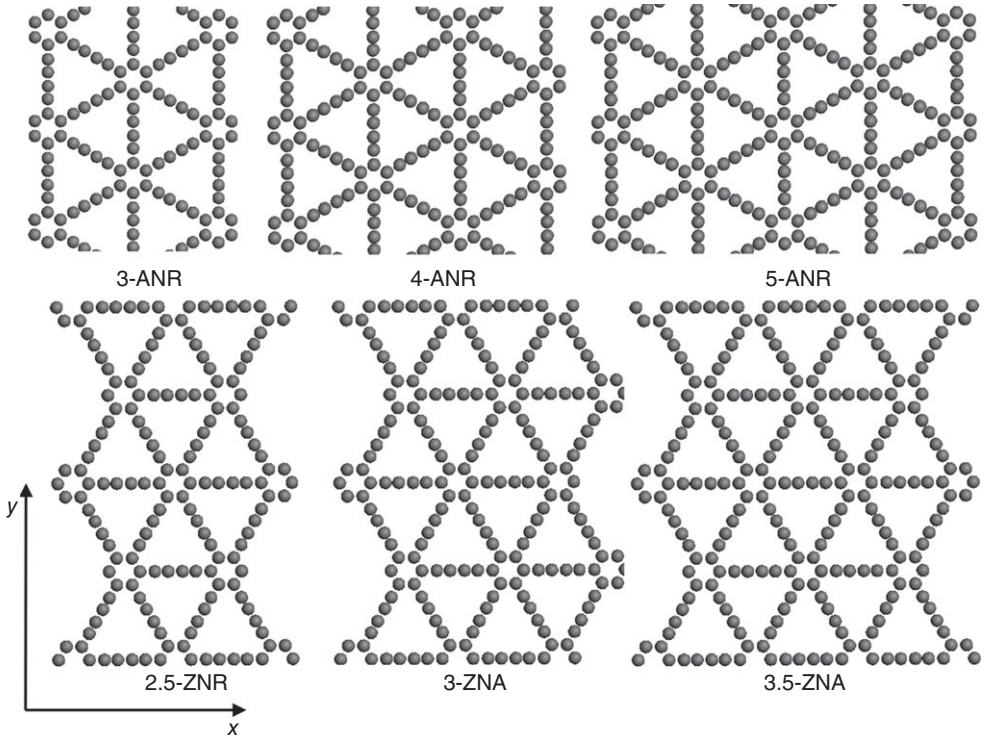

FIGURE 5 | Structures of armchair nanoribbon (ANR) and zigzag nanoribbon (ZNR) for graphdiynes (GDY) with different widths (number of C_6 hexagons).

from 0.5 to 1.3 eV. The similar results for GDY NRs were obtained by using the PBE functional with the band gaps in the range of 0.48–1.54 eV, depending on the width and edge morphology.[21]

The band gaps of GDY NRs can be further tuned by applying a transverse electric field,[23] with the band gap decreasing upon increasing the electric field strength; and for certain electric field strengths, a semiconductor to metal transition is predicted, which is caused by the localization of near-Fermi states induced by the electric field. Recently, the spontaneous magnetization of α-GY NRs was reported.[34] The results show that all ANRs behave as nonmagnetic semiconductors, while ZNRs become magnetic and adopt a ground state with ferromagnetic spin ordering at each edge and the opposite spin orientation between the edges, with magnetic moments depending on the width of the zigzag-like ribbons. As the zigzag graphene NRs will turn to half-metal by a transverse electric field,[35] the authors find that half-metal behavior of α-GY ZNRs may also be achieved by applying a transverse electric field.[34]

CHARGE CARRIER MOBILITY COMPUTATIONS

The primary interest for graphene is the expected high-charge mobility deriving from the Dirac cone structure, implying great applications in nanoelectronic and optoelectronic devices.[7,8] Experimentally, 2D GDY exhibits a conductivity of 2.516×10^{-4} Sm^{-1} at room temperature,[11] and 1D GDY nanowires exhibit high conductivity (1.9×10^{3} Sm^{-1}) and high mobility (7.1×10^{2} cm^2 V^{-1} second^{-1}) at room temperature.[12] Theoretical investigations of the electronic structures suggest that these graphene-like carbon allotropes could have excellent intrinsic charge transport properties comparable to graphene. In the following, we discuss the recent theoretical predictions on the carrier mobility in GYs and GDY.

Due to the delocalized nature of the electronic states, the Boltzmann transport theory with the relaxation time approximation[36] can be applied for calculating the carrier mobility in these carbon allotropes. In this context, the carrier mobility is expressed as[26]

$$\mu = \mathrm{e}\frac{\sum_i \int \left[\tau\left(i,\mathbf{k}\right)\mathbf{v}^2\left(i,\mathbf{k}\right)\right]\left(\partial f_{i\mathbf{k}}\right)/\left(\partial\varepsilon_{i\mathbf{k}}\right)\mathrm{d}\mathbf{k}}{\sum_i \int f_{i\mathbf{k}}\mathrm{d}\mathbf{k}}, \quad (1)$$

where i is the band index and $\mathbf{k}$ is the wave vector of electron, $f_{i\mathbf{k}}$ is the Fermi–Dirac distribution function. $\mathbf{v}(i,\mathbf{k})=[(1/\hbar)\nabla_{\mathbf{k}}\varepsilon_{i\mathbf{k}}]$ is the group velocity of electron. The electron scattering rate is defined as[37]

$$\frac{1}{\tau\left(i,\mathbf{k}\right)} = \frac{2\pi}{\hbar}\sum_{j\mathbf{q}\lambda}\left|g^{\lambda}_{ji}\left(\mathbf{k},\mathbf{q}\right)\right|^2\{\left[f_{j\mathbf{k}+\mathbf{q}}+n_{\mathbf{q}\lambda}\right]\delta\left(\varepsilon_{j\mathbf{k}+\mathbf{q}}-\varepsilon_{i\mathbf{k}}-\hbar\omega_{\mathbf{q}\lambda}\right) + \left[1+n_{\mathbf{q}\lambda}-f_{j\mathbf{k}+\mathbf{q}}\right]\delta\left(\varepsilon_{j\mathbf{k}+\mathbf{q}}-\varepsilon_{i\mathbf{k}}+\hbar\omega_{\mathbf{q}\lambda}\right)\}, \quad (2)$$

where $\tau(i,\mathbf{k})$ is the electron scattering time, $\varepsilon_{i\mathbf{k}}$ is the band energy of electron, $n_{\mathbf{q}\lambda}$ is the Bose–Einstein distribution function of phonon with the phonon mode λ and wave vector $\mathbf{q}$. The first and second δ functions describe the absorption and emission of a phonon $\omega_{\mathbf{q}\lambda}$. $g^{\lambda}_{ji}\left(\mathbf{k},\mathbf{q}\right)$ is the EPC matrix element,

$$g^{\lambda}_{ji}\left(\mathbf{k},\mathbf{q}\right) = \sqrt{\frac{\hbar}{2M\omega_{\mathbf{q}\lambda}}}\left\langle\psi_{j\mathbf{k}+\mathbf{q}}\right|\Delta_{\mathbf{q}\lambda}V\left|\psi_{i\mathbf{k}}\right\rangle, \quad (3)$$

which describes the transition rate for electron from one state $(i,\mathbf{k})$ to another state $(j,\mathbf{k}+\mathbf{q})$ scattered by a phonon $(\lambda,\mathbf{q})$. Here M is the atomic mass in the unit cell and $\Delta_{\mathbf{q}\lambda}V$ is the derivative of the potential with respect to the atomic displacement associated with the phonon mode λ and wave vector $\mathbf{q}$. Therefore, the key issue for the prediction of intrinsic carrier mobility is to determine the EPCs. Two methods, including DP theory[38] and DFPT,[39] have been applied to determine the EPCs in GYs and GDY.

Prediction Based on Deformation Potential Theory

A simple model for obtaining the EPCs is based on the DP theory, which was proposed by Bardeen and Shockley.[38] Following their argument, the dominant scattering of a thermal electron or hole arises mostly from the longitudinal acoustic (LA) phonons, as the electron coherence length is close to the acoustic phonon wavelength and much longer than the bond length. This is expected to be the case for GYs and GDY due to their covalently bonded conjugated structures like graphene. Actually, the DP model has been successfully applied for carbon materials,[21,22,27,40] DNA stacks,[41] and small conjugated organic molecules.[26,42,43] The DP theory assumes that the lattice potential perturbation due to thermal motions $\Delta V(\mathbf{r})$ has a linear dependence on the relative volume change $\Delta(\mathbf{r})$. Namely, $\Delta V(\mathbf{r})=D_{\mathrm{LA}}\Delta(\mathbf{r})$, where D_{LA} is defined as the LA DP constant. Finally, the thermally average EPC matrix element becomes[26]

$$\left\langle\left|\left\langle\psi_{i\mathbf{k}}\right|\Delta V\left|\psi_{i\mathbf{k}'}\right\rangle\right|^2\right\rangle = \frac{k_{\mathrm{B}}T\left(D^{i}_{\mathrm{LA}}\right)^2}{C}, \quad (4)$$

where we assume that the matrix element is independent of $\mathbf{k}$ or $\mathbf{k}'$. D^{i}_{LA} is the LA DP constant of the i-th band and C is the elastic constant. Both parameters can be derived from first principles by lattice deformation. The electron scattering time by the LA phonons can be expressed as[26]

$$\frac{1}{\tau\left(i,\mathbf{k}\right)} = \frac{2\pi k_{\mathrm{B}}T\left(D^{i}_{\mathrm{LA}}\right)^2}{\hbar C}\sum_{\mathbf{k}'}\delta\left(\varepsilon_{i\mathbf{k}}-\varepsilon_{i\mathbf{k}'}\right)\left(1-\frac{v_{i\mathbf{k}'}}{v_{i\mathbf{k}'}}\right). \quad (5)$$

The δ function suggests the LA phonon scattering is a quasi-elastic scattering. For computational details, we refer readers to Ref 26.

GDY and Its NRs

We have predicted the carrier mobility of GDY according to Equations (1) and (5).[22] It is found that the mobility of GDY is smaller than that of graphene at room temperature, but still as high as 10^5 cm^2 V^{-1} second^{-1}, showing excellent transport properties. The smaller mobility for GDY may come from its small elastic constant, compared to

TABLE 2 | Band Gap E_{gap}, Effective Mass m_h* and m_e*, DP Constant D_h and D_e, 1D Elastic Constant C_{1D} and Mobility μ_h and μ_e at Room Temperature (300 K) for Five GDY NRs (Reprinted with permission from Ref 22. Copyright 2011 American Chemical Society)

NR	E_{gap} (eV)	m_h* (m_0)	m_e* (m_0)	D_h (eV)	D_e (eV)	C_{1D} (eV cm^{-1})	μ_h (cm^2 V^{-1} second^{-1})	μ_e (cm^2 V^{-1} second^{-1})
2-ANR	0.954	0.086	0.081	7.406	2.006	1.244×10^4	0.711×10^3	10.580×10^3
3-ANR	0.817	0.087	0.086	6.790	1.730	1.864×10^4	1.253×10^3	19.731×10^3
2-ZNR	1.205	0.216	0.281	4.386	1.972	1.035×10^4	0.426×10^3	1.418×10^3
2.5-ZNR	1.015	0.174	0.207	4.776	2.054	1.420×10^4	0.679×10^3	2.829×10^3
3-ZNR	0.895	0.149	0.174	4.786	2.000	1.787×10^4	1.073×10^3	5.015×10^3

DP, deformation potential; GDY NRs, graphdiynes nanoribbons; ANR, armchair nanoribbons; ZNR, zigzag nanoribbons.

graphene. Further, we have also examined the carrier mobility in GDY NRs based on the effective mass approximation.[22] With the DP theory and effective mass approximation, the carrier mobility of 1D system can be expressed as[22]

$$\mu = \frac{e\hbar^2 C}{(2\pi k_B T)^{1/2} |m^*|^{3/2} D_{LA}^2} \quad (6)$$

where $m^* = \hbar^2/[\partial^2\varepsilon(\mathbf{k})/\partial\mathbf{k}^2]$ is the effective mass of charge carrier. Five types of GDY NRs (2-ANR, 3-ANR, 2-ZNR, 2.5-ZNR, and 3-ZNR) have been studied; the calculated electronic property and transport parameters at room temperature (300 K) are listed in Table 2. It is noted that (1) the band gap decreases as the width of NR increases, irrespective of the edge morphology; (2) the effective masses of electron and hole for ANRs are smaller than those for ZNRs; (3) the mobility increases slightly with the width among the same class of GDY NRs; (4) the mobility for ANRs is larger than that for ZNRs, especially for electrons, when the width of ribbons is similar; (5) the electron mobility is larger than the hole mobility in all GDY NRs, and the largest electron mobility by our prediction can reach 10^4 cm^2 V^{-1} second^{-1} at room temperature. We noticed that Huang and coworkers.[21] also discussed the carrier mobility of 1D GDY NRs based on the DP theory and effective mass approximation. They studied 12 ANRs and ZNRs of GDY, respectively, and found that the mobility of GDY NRs increases with their width and the highest mobility is 10^6 cm^2 V^{-1} second^{-1} at room temperature. For comparison, the mobilities of GDY NRs from Refs 21 and 22 have both been plotted in Figure 6. It is found that the results from two studies are close to each other.

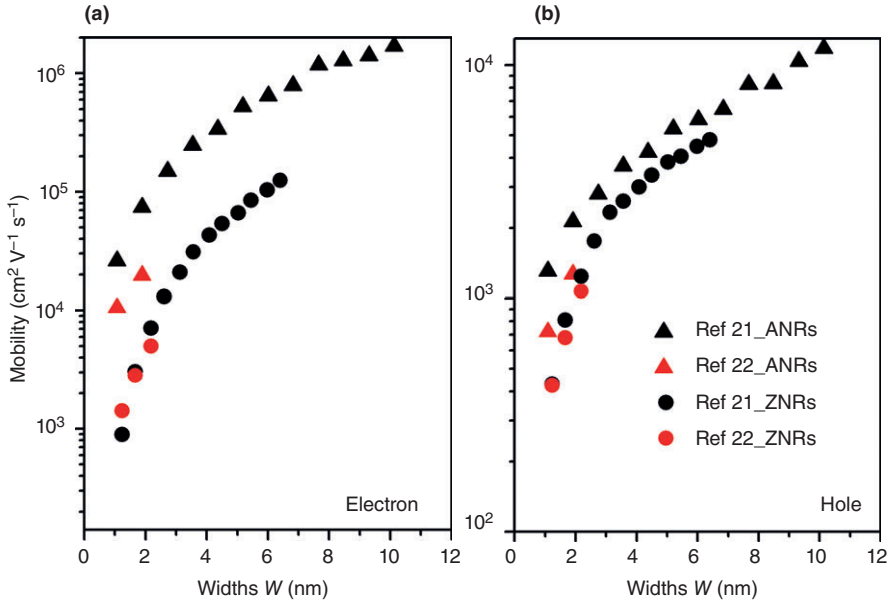

FIGURE 6 | Calculated mobilities of (a) electron and (b) hole for graphdiynes nanoribbons (GDY NRs) with different widths at room temperature (300 K) from Ref 21 (black symbols) and Ref 22 (red symbols), respectively. (Reprinted with permission from Ref 21. Copyright 2011 The Royal Society of Chemistry; Ref 22. Copyright 2011 American Chemical Society)

TABLE 3 | 2D Elastic Constant C_{2D}, DP Constant D, Carriers Scattering Time τ_h and τ_e, and Mobility μ_h and μ_e at Room Temperature (300 K) for α-, β-, and 6,6,12-GYs, as Well as Graphene (Reprinted with permission from Ref 27. Copyright 2013 American Chemical Society)

Carbon Allotropes	Acetylenic Linkage (%)	Axis	C_{2D} (J m^{-2})	D (eV)	τ_h (picoseconds)	τ_e (picoseconds)	μ_h (cm^{-1} V^{-1} second^{-1})	μ_e (cm^{-1} V^{-1} second^{-1})
α-GY	100	*a*	94.30	2.94	2.84	2.83	3.316×10^4	3.327×10^4
		b	95.19	2.97	2.80	2.79	2.960×10^4	2.716×10^4
β-GY	66.67	*a*	131.41	2.99	5.82	6.40	1.076×10^4	0.892×10^4
		b	130.65	3.11	5.37	5.91	0.856×10^4	0.798×10^4
6,6,12-GY	41.67	*a*	199.37	3.07	12.31	17.75	42.92×10^4	54.10×10^4
		b	150.52	3.56	6.93	9.99	12.29×10^4	24.48×10^4
Graphene	0	*a*	328.02	5.14	13.80	13.94	32.17×10^4	33.89×10^4
		b	328.30	5.00	13.09	13.22	35.12×10^4	32.02×10^4

DP, deformation potential; GY, graphyne.
a (*b*) axis is perpendicular (parallel) to C—C bond direction.

The above theoretical results suggest that the carrier mobility in 2D GDY sheet can reach about 10^5 cm^2 V^{-1} second^{-1} at room temperature, and we can modulate the carrier mobility of GDY NRs through their width and edge morphology.

Graphynes

The existence of Dirac cones indicates that the intrinsic carrier mobility of GYs might be as high as that of graphene. Inspired by the new discovery of Dirac cones in GYs, in 2013 we predicted the intrinsic carrier mobility of α-, β-, and 6,6,12-GYs based on the first-principle band structure calculations and the Boltzmann transport equation under the DP theory.[27] The DP constants, elastic constants, scattering times, and carrier mobilities at 300 K of GYs are summarized in Table 3. The corresponding values of graphene are also provided for comparison.

It can be seen from Table 3 that (1) the elastic constant of GY decreases as the percentage of acetylenic linkages increases because the presence of the linkages makes GYs less rigid; (2) the scattering time decreases as the percentage of acetylenic linkages increases from 41.67% for 6,6,12-GY to 100% for α-GY; (3) the intrinsic carrier mobility of 6,6,12-GY at room temperature can reach 5.41×10^5 and 4.29×10^5 cm^2 V^{-1} second^{-1} for electrons and holes, respectively, which are larger than those of graphene. According to Equations (1) and (5), the intrinsic carrier mobilities rely not only on the EPCs, but also on the group velocities and the shapes of the Fermi surface. 6,6,12-GY features two inequivalent Dirac cones, and the carriers in it behave like the Dirac fermions traveling at a speed of light, as in graphene. The high carrier mobility of 6,6,12-GY can be attributed to (1) weaker EPC strength; (2) two inequivalent Dirac cones in the Brillouin zone.

Our theoretical calculations predicted that the carrier mobilities in 6,6,12-GY could be even larger than those of graphene and hint that hybridization of sp–sp^2 carbon may be capable of improving the transport behaviors of the carbon allotropes through lowering the electron–phonon scatterings. Band structure engineering provides a clue for tuning charge transport in 2D carbon materials.

Prediction Based on Density Functional Perturbation Theory

The DP theory has been widely used in studying the carrier transport in carbon materials as we discussed above. However, only LA phonon scattering is considered in DP theory. The key parameter DP constant derived in different ways showed large variations, such as 5.14,[26] 29,[44] and 4.5 eV[45] in graphene. The optical phonon scatterings, which are absent in the DP theory, have been shown to play an important role in carrier scatterings of 2D MoS_2 at room temperature.[46] Thus, theoretical analysis of EPCs contributed by different phonon modes with phonon dispersions beyond the DP theory is clearly called for.

DFPT is a powerful tool to obtain the vibrational properties and EPCs with the phonon dispersion and the corresponding normal modes from the first-principle inter-atomic force constants.[39] This method has now been used to study the EPCs in silicon,[47] monolayer,[45] and bilayer graphene,[48] etc. But it remains challenging to fully address the carrier scatterings with all phonon modes and dispersions. Recently, based on DFPT, determination of EPCs for complex solids becomes possible on fine grids in the Brillouin zone for both electron and phonon states by utilizing the Wannier-Fourier interpolation method.[49] Following these methods, we have given an in-depth

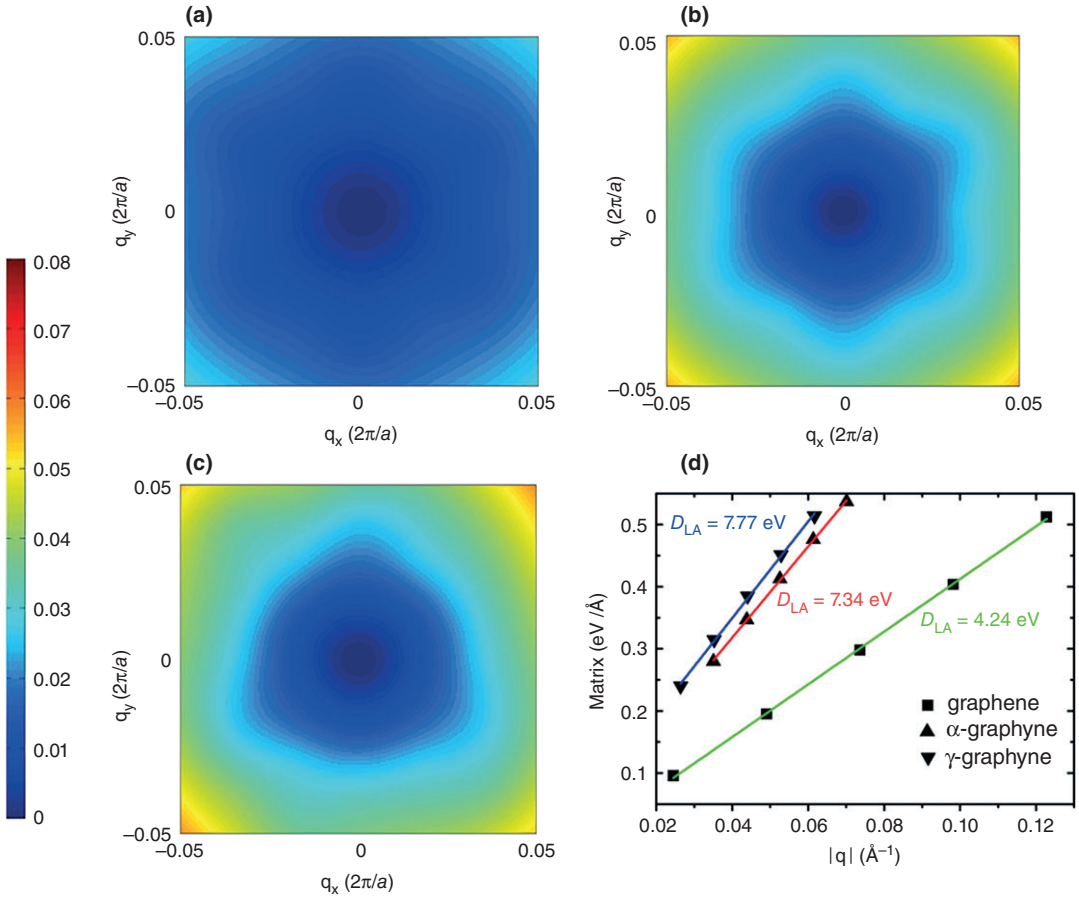

FIGURE 7 | Contour plots showing the square of e-ph coupling matrix elements $\left|g_{ji}^{\lambda}(\mathbf{k},\mathbf{q})\right|^2$ (in eV^2) calculated by density functional perturbation theory (DFPT) and Wannier-interpolation for (a) graphene, (b) α-graphyne (GY) and (c) γ-GY, as a function of longitudinal acoustic (LA) phonon wave vector **q** (near the center of the Brillouin zone). **k** is at the conduction band (CB) minimum (**K**-point for graphene and α-GY, **M**-point for γ-GY) and the initial *i* and final *j* electronic states are both limited to the CB. (d) The matrix element of LA phonon scattering as a function of phonon wave vector **q** in the long-wavelength limit. The slope is the LA deformation potential (DP) constant. (Reprinted with permission from Ref 50. Copyright 2014 AIP Publishing LLC)

discussion of the EPCs and carrier transport in α- and γ-GYs.[50] For comparison, EPCs in graphene have also been studied.

Figure 7(a)–(c) depicts the square of EPC matrix elements in Equation (3) as a function of the LA phonon wave vector **q** (near the center of Brillouin zone) for graphene, α-, and γ-GYs, respectively. The electronic states (both initial and final states for scatterings) are limited to the conduction band (CB) (the electronic wave vector **k** is in the **K**-valley for graphene and α-GY, but in the **M**-valley for γ-GY). The scattering matrix elements manifest clear isotropy near the center of Brillouin zone. In DP theory, for scattering with acoustic phonons in the long-wavelength limit, the matrix element is linear in $|\mathbf{q}|$[51]

$$M_{ii}^{\mathrm{LA}}(\mathbf{k},\mathbf{q}) = \left\langle \psi_{i,\mathbf{k}+\mathbf{q}} \middle| \Delta_{\mathbf{q},\mathrm{LA}} V \middle| \psi_{i,\mathbf{k}} \right\rangle = D_{\mathrm{LA}} |\mathbf{q}|, \quad (7)$$

where D_{LA} is the LA DP constant. According to Equation (7), the LA DP constants of graphene, α-, and γ-GYs are obtained by a linear fitting of the matrix element at $|\mathbf{q}| \to 0$, as shown in Figure 7(d). It is found that the LA DP constant of graphene is 4.24 eV, which is close to others' first-principle calculations of the effective acoustic DP constants (e.g., 4.5[45] and 6.8 eV[52] by direct lattice dynamics calculations). This value is also in agreement with the result (5.14 eV[26]) obtained with the DP theory, by a linear fitting of the band edge shift with respect to the unit cell dilation. The LA DP constants for α-GYs (7.34 eV) and γ-GYs (7.77 eV) are larger than that of graphene, suggesting stronger LA phonon scatterings in α- and γ-GYs.

According to Equation (2), the scattering times of an electron at the CB minimum by four most important in-plane phonon modes, transverse acoustic (TA),

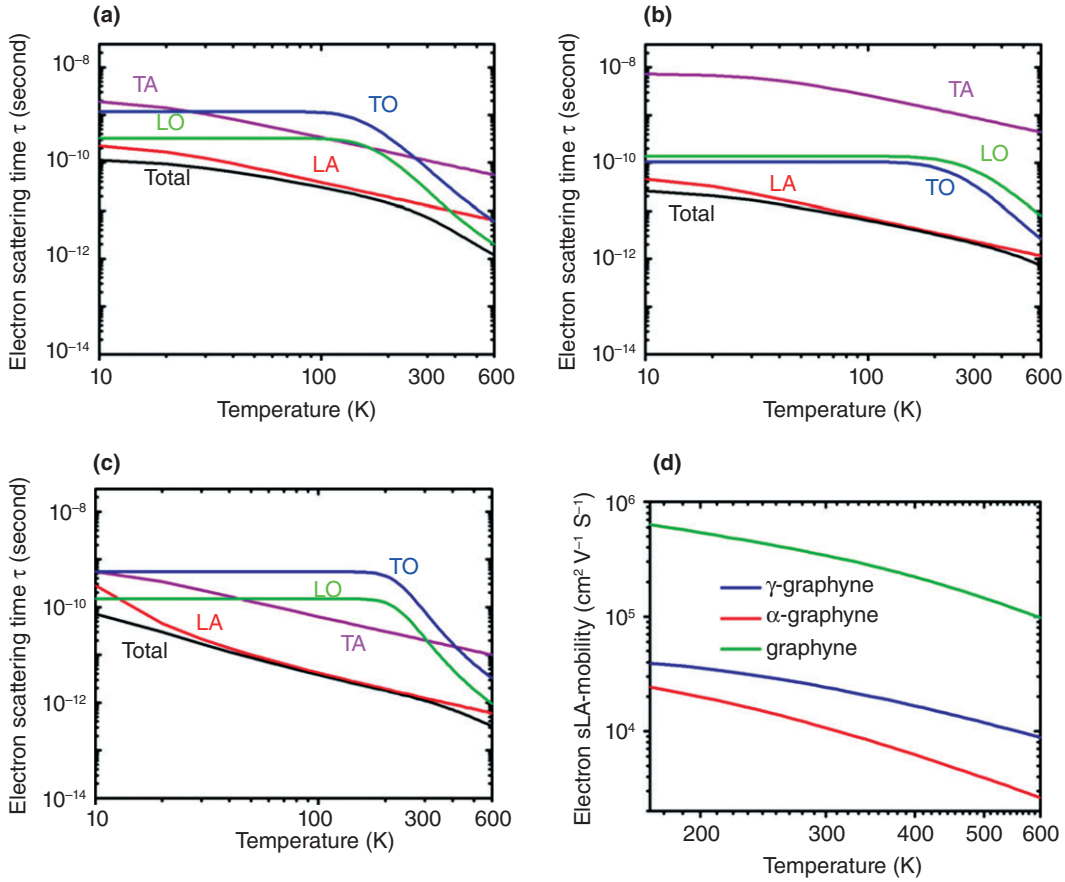

FIGURE 8 | (a), (b) and (c) are the scattering times of an electron at the conduction band (CB) minimum by different phonon modes as a function of temperature for graphene, α-graphyne (GY), and γ-GY. (d) Electron mobility limited by longitudinal acoustic (LA) phonon scattering as a function of temperature for these systems. (Reprinted with permission from Ref 50. Copyright 2014 AIP Publishing LLC)

longitudinal acoustic (LA), transverse optical (TO), and longitudinal optical (LO) modes, as a function of temperature are shown in Figure 8(a)–(c) for graphene, α-, and γ-GYs, respectively. The total scattering times are also plotted in these figures based on Matthiessen's rule. It indicates that (1) the electron scattering time by LA phonon at room temperature (300 K) for both graphene (~10 picoseconds) and α-GY (~2 picoseconds) is in good agreement with our previous works based on the DP theory (13.9 picoseconds for graphene, 2.8 picoseconds for α-GY)[27]; (2) the LA phonon scattering is the main scattering mechanism over a large range of temperatures for these systems, even at room temperature, resulting from its strong coupling strength; (3) at low temperatures, due to the few excitation of high-frequency optical phonons, the optical phonon scattering is suppressed and the electron scattering time by optical phonon remains almost unchanged with temperature; (4) the optical phonon scattering should not be neglected at high temperatures, due to the increasing number of optical phonons and significant coupling strength, especially for graphene, where the scattering time curves of LA and LO exhibit a crossover at around 400 K.

Finally, the predicted carrier mobilities of both α- and γ-GYs are on the order of 10^4 cm^2 V^{-1} second^{-1} at room temperature, according to Equation (1). The electron mobilities by LA phonon scattering for graphene, α-, and γ-GYs, as a function of temperature, are shown in Figure 8(d). The lower mobilities of α- and γ-GYs compared with graphene are due to the stronger LA phonon scatterings of GYs. Conveniently, the carrier scattering times and mobilities by different phonon modes at room temperature are summarized in Table 4 for these systems.

The application of DFPT combined with Wannier-Fourier interpolation method to 2D carbon materials elucidates that the main scattering mechanism in these 2D carbon materials is the LA phonon scattering, but the optical phonon scattering can play an important role at high temperatures, especially for graphene.

TABLE 4 | The Carriers Scattering Times and Mobilities with Different Phonon Scattering Mechanisms for Graphene, α-, and γ-graphynes (GYs) at Room Temperature (300 K) (Reprinted with permission from Ref 50. Copyright 2014 AIP Publishing LLC)

		Graphene		α-GY		γ-GY	
	Phonon Mode	Hole	Electron	Hole	Electron	Hole	Electron
τ (picoseconds)	LA	14.28	12.78	2.17	2.33	0.56	1.25
	TA	161.32	111.46	711.64	882.80	16.30	20.27
	LO	27.78	26.43	68.74	70.06	17.07	22.61
	TO	74.98	76.02	33.57	34.29	59.19	79.78
	Total	7.97	7.24	1.97	2.11	0.52	1.10
μ (10^4 cm^2 V^{-1} second^{-1})	LA	41.38	34.12	0.99	1.07	0.39	2.42
	TA	591.81	304.75	314.66	380.06	7.30	13.04
	LO	82.43	78.22	73.41	75.12	7.61	10.05
	TO	218.06	222.53	59.16	59.70	27.82	37.81
	Total	23.49	20.05	0.96	1.03	0.35	1.62

The total scattering times and mobilities are also obtained with Matthiessen's rule.

TABLE 5 | The LA DP Constant D_{ac}, 2D Elastic Constant C_{2D}, the Carrier Scattering Time τ_h and τ_e, and Mobility μ_h and μ_e at Room Temperature (300 K) for Graphene by Using DP Theory (Ref 26) and DFPT (Ref 50), Respectively, Along the Direction Perpendicular ($\perp$) or Parallel ($\parallel$) to C—C Bond

	Direction	D_{ac} (eV)	C_{2D} (J m^{-2})	τ_h (picoseconds)	τ_e (picoseconds)	μ_h (cm^{-1} V^{-1} second^{-1})	μ_e (cm^{-1} V^{-1} second^{-1})
DP	$\perp$C–C	5.14	328.02	13.80	13.94	32.2×10^4	33.9×10^4
	$\parallel$C–C	5.00	328.30	13.09	13.22	35.1×10^4	32.0×10^4
DFPT	$\parallel$C–C	4.24	364.47	14.28	12.78	41.38×10^4	34.12×10^4

LA, longitudinal acoustic; DP, deformation potential; DFPT, density functional perturbation theory.

Comparison Between DP and DFPT

Finally, the transport properties obtained with the two methods, DP theory and DFPT, taking graphene as an example, are summarized in Table 5. It is found that the results obtained by the two methods are similar, for instance, the scattering time τ_h is ~13 picoseconds by DP theory and ~14 picoseconds by DFPT, and the mobility μ_h is $\sim3\times10^5$ cm^{-1} V^{-1} second^{-1} by DP theory and $\sim4\times10^5$ cm^{-1} V^{-1} second^{-1} by DFPT in graphene. The DP constants along different directions are close to each other, showing the isotropy of EPCs near the Brillouin zone center. Thus, the main phonon scattering responsible for charge transport is long-wavelength LA phonon, and the DP theory is suitable for calculating EPCs in these carbon systems.

CONCLUSION

In this overview, we outlined the most recent theoretical predictions on the electronic properties and charge carrier mobilities of GYs and GDYs. Both DP theory and DFPT have been applied to determine EPCs in GYs and GDYs. The first-principle electronic structure calculations indicate that γ-GY and GDY are semiconductors, while α-, β-, and 6,6,12-GYs are semimetals with Dirac cones. The band gaps of GYs and GDY are tunable in various ways, such as straining, cutting into NRs with different widths and edge morphology, applying external electric fields. Based on the Boltzmann transport equation and DP theory, the predicted carrier mobility for both GYs and GDY can reach as high as 10^4–10^5 cm^2 V^{-1} second^{-1} at room temperature, and for 6,6,12-GY, which has two inequivalent Dirac cones, the carrier mobility is even larger than graphene. Besides, through analyzing the EPCs with DFPT and Wannier-interpolation technique, it is found that the main scattering mechanism in these carbon allotropes over a wide range of temperatures ($\leq$300 K) is the LA phonon scattering, but the optical phonon scattering should not be neglected at high temperatures (>300 K). These results suggest that the sp^1+sp^2 hybridized carbon allotropes can compete with conventional sp^2 carbon systems such as fullerenes, nanotubes, and graphene, and are promising materials for electronic and optoelectronic applications.

Nevertheless, challenges remain in the field of carbon nanomaterials. First of all, the exceptional performances have been predicted only by theory, and the

realization is still on the way. Although the potential utilizations of various exotic properties of GYs and GDY have been foreseen, the preparation techniques of these low-dimensional carbon allotropes with large area, high quality, and stability are yet to be developed. Secondly, new carbon allotropes await to be discovered (such as graphone, graphane, nanotoroids, and nanocones),[28] and their structure–property relationship remains to be understood. So, efforts from both experimental and theoretical communities are needed for practical applications of these new carbon materials.

ACKNOWLEDGMENTS

This work is supported by the National Natural Science Foundation of China (Grant Nos 21273124 and 21290190) and the Ministry of Science and Technology of China (Grant Nos 2011CB932304, 2011CB808405, and 2013CB933503).

REFERENCES

1. Kratschmer W, Lamb LD, Fostiropoulos K, Huffman DR. Solid C60: a new form of carbon. *Nature* 1990, 347:354–358.
2. Iijima S. Helical microtubules of graphitic carbon. *Nature* 1991, 354:56–58.
3. Novoselov KS, Geim AK, Morozov SV, Jiang D, Zhang Y, Dubonos SV, Grigorieva IV, Firsov AA. Electric field effect in atomically thin carbon films. *Science* 2004, 306:666–669.
4. Taylor R, Walton DRM. The chemistry of fullerenes. *Nature* 1993, 363:685–693.
5. Wong SS, Joselevich E, Woolley AT, Cheung CL, Lieber CM. Covalently functionalized nanotubes as nanometre- sized probes in chemistry and biology. *Nature* 1998, 394:52–55.
6. Geim AK. Graphene: status and prospects. *Science* 2009, 324:1530–1534.
7. Li Y, Xu L, Liu H, Li Y. Graphdiyne and graphyne: from theoretical predictions to practical construction. *Chem Soc Rev* 2014, 43:2572–2586.
8. Ivanovskii AL. Graphynes and graphdyines. *Prog Solid State Chem* 2013, 41:1–19.
9. Baughman R, Eckhardt H, Kertesz M. Structure-property predictions for new planar forms of carbon: layered phases containing sp and sp atoms. *J Chem Phys* 1987, 87:6687.
10. Haley MM, Brand SC, Pak JJ. Carbon networks based on dehydrobenzoannulenes: synthesis of graphdiyne substructures. *Angew Chem Int Ed Engl* 1997, 36:836–838.
11. Li G, Li Y, Liu H, Guo Y, Li Y, Zhu D. Architecture of graphdiyne nanoscale films. *Chem Commun* 2010, 46:3256–3258.
12. Qian X, Ning Z, Li Y, Liu H, Ouyang C, Chen Q, Li Y. Construction of graphdiyne nanowires with high-conductivity and mobility. *Dalton Trans* 2012, 41:730–733.
13. Luo G, Qian X, Liu H, Qin R, Zhou J, Li L, Gao Z, Wang E, Mei WN, Lu J, et al. Quasiparticle energies and excitonic effects of the two-dimensional carbon allotrope graphdiyne: theory and experiment. *Phys Rev B* 2011, 84:075439.
14. Narita N, Nagai S, Suzuki S, Nakao K. Optimized geometries and electronic structures of graphyne and its family. *Phys Rev B* 1998, 58:11009–11014.
15. Jiao Y, Du A, Hankel M, Zhu Z, Rudolph V, Smith SC. Graphdiyne: a versatile nanomaterial for electronics and hydrogen purification. *Chem Commun* 2011, 47:11843–11845.
16. Enyashin AN, Ivanovskii AL. Graphene allotropes. *Phys Status Solidi B* 2011, 248:1879–1883.
17. Malko D, Neiss C, Viñes F, Görling A. Competition for graphene: graphynes with direction-dependent Dirac cones. *Phys Rev Lett* 2012, 108:086804.
18. Cui HJ, Sheng XL, Yan QB, Zheng QR, Su G. Strain-induced Dirac cone-like electronic structures and semiconductor-semimetal transition in graphdiyne. *Phys Chem Chem Phys* 2013, 15:8179–8185.
19. Yue Q, Chang S, Kang J, Qin S, Li J. Mechanical and electronic properties of graphyne and its family under elastic strain: theoretical predictions. *J Phys Chem C* 2013, 117:14804–14811.
20. Pan LD, Zhang LZ, Song BQ, Du SX, Gao HJ. Graphyne- and graphdiyne-based nanoribbons: density functional theory calculations of electronic structures. *Appl Phys Lett* 2011, 98:173102.
21. Bai H, Zhu Y, Qiao W, Huang Y. Structures, stabilities and electronic properties of graphdiyne nanoribbons. *RSC Adv* 2011, 1:768–775.
22. Long MQ, Tang L, Wang D, Li YL, Shuai ZG. Electronic structure and carrier mobility in graphdiyne sheet and nanoribbons: theoretical predictions. *ACS Nano* 2011, 5:2593–2600.

23. Kang J, Wu FM, Li JB. Modulating the bandgaps of graphdiyne nanoribbons by transverse electric fields. *J Phys Condens Matter* 2012, 24:165301.
24. Zheng Q, Luo G, Liu Q, Quhe R, Zheng J, Tang K, Gao Z, Nagase S, Lu J. Structural and electronic properties of bilayer and trilayer graphdiyne. *Nanoscale* 2012, 4:3990–3996.
25. Leenaerts O, Partoens B, Peeters FM. Tunable double Dirac cone spectrum in bilayer α-graphyne. *Appl Phys Lett* 2013, 103:013105.
26. Xi JY, Long MQ, Tang L, Wang D, Shuai ZG. First-principles prediction of charge mobility in carbon and organic nanomaterials. *Nanoscale* 2012, 4:4348–4369.
27. Chen JM, Xi JY, Wang D, Shuai ZG. Carrier mobility in graphyne should be even larger than that in graphene: a theoretical prediction. *J Phys Chem Lett* 2013, 4:1443–1448.
28. Peng Q, Dearden AK, Crean J, Han L, Liu S, Wen X, De S. New materials graphyne, graphdiyne, graphone, and graphane: review of properties, synthesis, and application in nanotechnology. *Nanotechnol Sci Appl* 2014, 7:1–29.
29. Andrew RC, Mapasha RE, Ukpong AM, Chetty N. Mechanical properties of graphene and boronitrene. *Phys Rev B* 2012, 85:125428.
30. Srinivasu K, Ghosh SK. Graphyne and graphdiyne: promising materials for nanoelectronics and energy storage applications. *J Phys Chem C* 2012, 116:5951–5956.
31. Narita N, Nagai S, Suzuki S, Nakao K. Electronic structure of three-dimensional graphyne. *Phys Rev B* 2000, 62:11146–11151.
32. Luo GF, Zheng QY, Mei WN, Lu J, Nagase S. Structural, electronic, and optical properties of bulk graphdiyne. *J Phys Chem C* 2013, 117:13072–13079.
33. Terrones M, Botello-Méndez AR, Campos-Delgado J, López-Urías F, Vega-Cantú YI, Rodríguez-Macías FJ, Elías AL, Muñoz-Sandoval E, Cano-Márquez AG, Charlier J-C, et al. Graphene and graphite nanoribbons: morphology, properties, synthesis, defects and applications. *Nano Today* 2010, 5:351–372.
34. Yue Q, Chang S, Kang J, Tan J, Qin S, Li J. Magnetic and electronic properties of α-graphyne nanoribbons. *J Chem Phys* 2012, 136:244702.
35. Son YW, Cohen ML, Louie SG. Half-metallic graphene nanoribbons. *Nature* 2006, 444:347–349.
36. Ziman JW. *Principles of the Theory of Solids*. 2nd ed. London: Cambridge University Press; 1972.
37. Grimvall G. *The Electron-Phonon Interaction in Metals, Selected Topics in Solid State Physics*. Amsterdam: North-Holland; 1981.
38. Bardeen J, Shockley W. Deformation potentials and mobilities in non-polar crystals. *Phys Rev* 1950, 80:72–80.
39. Baroni S, de Gironcoli S, Dal Corso A, Giannozzi P. Phonons and related crystal properties from density-functional perturbation theory. *Rev Mod Phys* 2001, 73:515–562.
40. Long MQ, Tang L, Wang D, Wang LJ, Shuai ZG. Theoretical predictions of size-dependent carrier mobility and polarity in graphene. *J Am Chem Soc* 2009, 131:17728–17729.
41. Beleznay FB, Bogár F, Ladik J. Charge carrier mobility in quasi-one-dimensional systems: application to a guanine stack. *J Chem Phys* 2003, 119:5690–5695.
42. Tang L, Long MQ, Wang D, Shuai ZG. The role of acoustic phonon scattering in charge transport in organic semiconductors: a first-principles deformation-potential study. *Sci China B Chem* 2009, 52:1646–1652.
43. Northrup JE. Two-dimensional deformation potential model of mobility in small molecule organic semiconductors. *Appl Phys Lett* 2011, 99:062111.
44. Bolotin KI, Sikes KJ, Hone J, Stormer HL, Kim P. Temperature-dependent transport in suspended graphene. *Phys Rev Lett* 2008, 101:096802.
45. Borysenko KM, Mullen JT, Barry EA, Paul S, Semenov YG, Zavada JM, Nardelli MB, Kim KW. First-principles analysis of electron-phonon interactions in graphene. *Phys Rev B* 2010, 81:121412.
46. Kaasbjerg K, Thygesen KS, Jacobsen KW. Phonon-limited mobility in n-type single-layer MoS_2 from first principles. *Phys Rev B* 2012, 85:115317.
47. Restrepo OD, Varga K, Pantelides ST. First-principles calculations of electron mobilities in silicon: phonon and Coulomb scattering. *Appl Phys Lett* 2009, 94:212103.
48. Borysenko KM, Mullen JT, Li X, Semenov YG, Zavada JM, Nardelli MB, Kim KW. Electron-phonon interactions in bilayer graphene. *Phys Rev B* 2011, 83:161402.
49. Giustino F, Cohen ML, Louie SG. Electron-phonon interaction using Wannier functions. *Phys Rev B* 2007, 76:165108.
50. Xi JY, Wang D, Yi YP, Shuai ZG. Electron-phonon couplings and carrier mobility in graphynes sheet calculated using the Wannier-interpolation approach. *J Chem Phys* 2014, 141:034704.
51. Ferry DK. *Semiconductor Transport*. New York: Taylor & Francis; 2000.
52. Kaasbjerg K, Thygesen KS, Jacobsen KW. Unraveling the acoustic electron-phonon interaction in graphene. *Phys Rev B* 2012, 85:165440.

